Int J Adv Manuf Technol (1997) 13:248–255
© 1997 Springer-Verlag London Limited

The International Journal of
Advanced
Manufacturing
Technology

Tool-Path Verification in Five-Axis Machining of Sculptured Surfaces

Chun-Fong You and Chih-Hsing Chu

Department of Mechanical Engineering, National Taiwan University, Taipei, Taiwan, ROC

This paper presents a systematic scheme for the verification of tool paths in five-axis machining of sculptured surfaces. The criterion of interference detection is developed for a general APT cutter. Tool interference problems which occur across multiple surfaces can be dealt with. In this work, sculptured surfaces are subdivided into discrete sample points for interference detection. The undetected interference error introduced in the surface subdivision process is ensured within a user-specified tolerance. Simulation results of test examples are included to demonstrate the feasibility of the proposed scheme.

Keywords: Five-axis machining; Interference detection; Sculptured surfaces; Tool-path verification

1. Introduction

Five-axis numerically controlled machining has been increasingly applied in manufacturing of mechanical parts since the late seventies. Compared with traditional three-axis machining, five-axis machining offers some advantages [1,2]. For instance, it can be used to deal with workpieces which contain overlapped surfaces because the tool motion has two additional degrees of freedom. The stepover between two adjacent tool paths is decreased, since the tool cutting end is able to match the shape of the machined surface [3]. In addition, machining preparatory work such as the exchange of jigs and fixtures is reduced. Therefore, the total manufacturing time from stock material to finished part can be greatly shortened by using five-axis NC machines. However, five-axis machining suffers from some problems. First, the precision of the machine dynamics needs to be improved because the simultaneous five-axis motion increases the machine volumetric errors [2]. The machine controller needs to be more sophisticated for NC data processing so that the machining tolerance can be ensured after interpolation of the tool paths [4]. In addition, tool interference frequently occurs in five-axis machining owing to the variable attitudes of the tool axes. Verification of tool paths in five-axis NC machining is sometimes conducted by trial cutting before the actual machining. The efficiency of five-axis machining is thus decreased.

Geometric modelling technology has been widely applied to mechanical design and manufacture, for example, in the development of computer-aided design (CAD) and computer-aided manufacturing (CAM). Geometric modelling technology offers many advantages from the initial design work to the final manufacturing and inspection process, especially for the production of parts with sculptured surfaces. Nowadays, the preparation of NC machining data is mostly carried out with the assistance of CAM systems. Five-axis NC machining inevitably uses CAM systems to finish the work, especially for tool-path generation [5], verification, simulation [6,7] and optimisation [8,9]. Some CAM systems provide dynamic simulation of tool paths for interference checking. However, the tool interference problems in five-axis machining may be complicated, especially when sculptured surfaces are machined. Not only can the cutting end of the tool induce overcuts of the machined surface, but the tool flank can also cause collisions with the other surfaces in the machining environment [10]. On visual verification of tool paths, some small tool collisions or interference which occur in overlapped surface regions cannot be found easily. Therefore, it is necessary to develop another tool-path verification method which is more reliable than visual-based methods.

2. Related Work

Some previous work has been done on the interference problems in NC machining, but most of it concentrates on gouge detection in three-axis machining. Choi and Jun [11] developed an algorithmic procedure that converts cutter contact (CC) data into interference-free cutter location (CL) data for a ball-end cutter in the three-axis NC machining of sculptured surfaces. Oliver [12] presented two techniques for gouge detection in three-axis sculptured surface NC program generation. Jerard et al. [13,14] developed surface-based techniques for the verification of three-axis NC programs used to machine sculptured surfaces. Surface curvature and cutting-tool size are used as

Correspondence and offprint requests to: Dr C. F. You, Department of Mechanical Engineering, National Taiwan University, 1 Roosevelt Road, Sec 4, Taipei 10764, Taiwan, R.O.C.

inputs to a surface discretisation algorithm, which allows a user-defined level of simulation accuracy to be achieved. Cutting errors can be shown as a colour graphics display in the simulation of the machining process. Chang and Goodman [6] presented a tool-path verification method for the multi-axis NC milling of sculptured surfaces. The method discretises the nominal sculptured surfaces and directly computes the possible interference between those discretised points on the surface and the moving tool without explicitly creating the boundary surface of the tool motion. Aretz [15] investigated cutter interference problems in three-axis machining. A surface discretisation method and its related data structure were presented to detect the interference regions in the machined surface. Some feasible strategies for tool-path corrections were evaluated for different interference cases. For five-axis machining with a flat-end cutter, Li and Jerard [5] presented an efficient algorithm for generating gouge-free tool paths for general sculptured surfaces.

In this paper, we present a systematic approach for tool-path verification in five-axis machining. Interference detection criterion is derived for the general APT cutter. The protected surfaces can ontain the machined surface and other neighbouring surfaces. First, the surface subdivision procedure developed by Jerard [14] is modified so that it can be applied to the interference problems caused by whole-tool geometry. The maximal undetected interference error can be ensured within a user-prescribed tolerance. Then the voxel model is established from the discrete sample points generated during the surface subdivision, and a method for finding the possible interfering cutter locations quickly is described. Finally, simulation results of test examples are included to demonstrate the feasibility of the proposed algorithms in tool-path verification for five-axis machining.

3. Surface Subdivision for Interference Detection

Sculptured surfaces are usually described by implicit parametric representations. Non-uniform rational B-splines (NURB) and Bézier polynomials are the most popular forms at present used in CAD/CAM systems. For tool-path verification, the problem can be considered an in/on/out test between the tool swept geometry and the protected surfaces [16]. It involves intersection calculation between these two geometry elements and requires intensive computation when the protected surfaces contain sculptured surfaces [7]. Therefore, it is not feasible for the direct in/on/out test to solve tool interference problems. Some modified approaches have been proposed to improve this situation. Most of them [6,14,17] use discrete approximation instead of the actual surface to detect interference. The computation time for interference detection depends on the degree of precision of the surface approximation. Additionally, the accuracy of interference detection is also strongly influenced by the deviation between the actual surface and its approximation. Hence, it is necessary to consider these two factors before the protected surfaces are subdivided.

A simple method for sculptured surface approximation is to take discrete points with constant *u*/*v* intervals from iso-parametric curves. Thus a polyhedral model of the sculptured surface that consists of those surface points can be obtained. As shown in Fig. 1, every two subsequent points $\mathbf{p}_1$, $\mathbf{p}_2$ of a *u* iso-parametric curve and corresponding point $\mathbf{p}_3$ of the next *u* iso-parametric curve compose a triangle in the polyhedral model, which is called a facet. A facet is considered to be the approximation of a small local surface region. Therefore, surface discretisation is sometimes labelled triangulation. By applying subdivision techniques, an approximate polyhedral can be very "close" to the nominal surface. Here, we must define the closeness of two geometric elements. Assume **a** and **b** are two points on a space curve **r**. Their geometric midpoint is $\mathbf{p}_g$ and their parametric midpoint is $\mathbf{p}_p$. Assume $\mathbf{a} = (a_x, a_y, a_z)$ and $\mathbf{b} = (b_x, b_y, b_z)$ and they can be represented by $\mathbf{a} = \mathbf{r}(u_a, v_a)$ and $\mathbf{b} = \mathbf{r}(u_b, v_b)$. Thus, $\mathbf{p}_g$ and $\mathbf{p}_p$ are expressed by

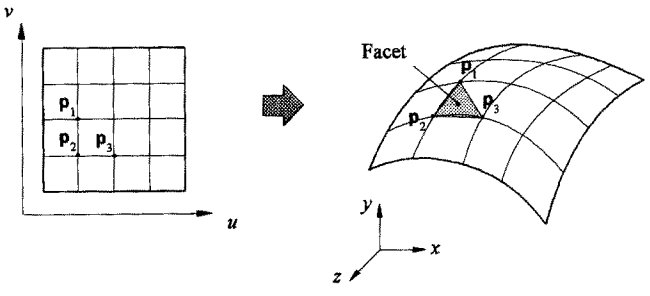

Fig. 1. Surface approximation with points on iso-parametric curves.

$$\mathbf{p}_g = \left(\frac{a_x + b_x}{2}, \frac{a_y + b_y}{2}, \frac{a_z + b_z}{2}\right),$$

$$\mathbf{p}_p = \mathbf{r}\left(\frac{u_a + u_b}{2}, \frac{v_a + v_b}{2}\right)$$

The distance between $\mathbf{p}_g$ and $\mathbf{p}_p$ is defined as the chordal deviation, as shown in Fig. 2. In this work, chordal deviation is considered to be the maximal error of approximation between a space curve segment and a line joining the two endpoints of the curve segment. For the approximation of a sculptured surface, the maximal deviation between the actual surface and its approximate facet is to be considered. There exists a maximal approximation error for each side on a facet. In addition, the deviation between the geometric and parametric midpoint of the facet is computed. The maximal value of these four errors is regarded as the approximation error of the facet.

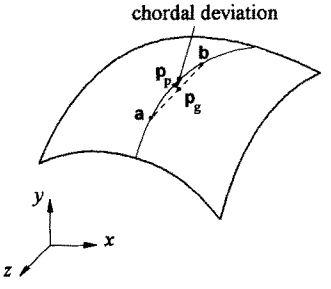

Fig. 2. Chordal deviations of a 3D curve segment.

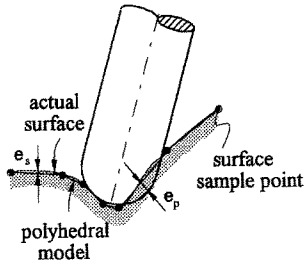

Fig. 3. Surface approximation error and tool protrusion error.

3.1 Undetected Error Analysis

The approximation of the actual surface causes errors when the interference detection is executed. The first error results from the deviation between the actual value and its approximation. We can ensure the chordal deviation within a user-specified tolerance by applying the surface subdivision method. The distributions of approximate points depend on surface curvatures. For example, the distance between two subsequent points along the axial direction is larger than it is along the circular direction when a cylindrical surface is discretisated. However, large distances between discrete points cause another error. As interference detection is applied only at discrete sample points, not for the polyhedral model, it is possible that the cutter does not interfere with the discrete sample points while it protrudes into the surface between the sample points, that is, interferes with the polyhedral model. Figure 3 illustrates two possible errors, defined as the surface approximation error e_s and the cutter protrusion error e_p. The maximal depth of an undetected overcut can be analysed in terms of e_s and e_p. The possible combinations of these two errors are shown in Fig. 4 [13]. In the worst case (see Fig. 4(*a*)), the two errors combine, so the subdivision must ensure that $e_s + e_p < e$, where e is the user-prescribed undetected error. If the approximate facet lies entirely outside the surface, the errors are in the same direction and cancel. Therefore, it is enough to ensure that $\max(e_s, e_p) < e$ (see Fig. 4(*b*) and 4(*c*)). If the maximum distance between the vertices of any facet is d, the maximal undetected cutter protrusion error e_p is conservatively approximated by [14]

$$d \sim \sqrt{(6re_p)} \tag{1}$$

Note that this equation is derived only for the cutting end of a ball-end cutter. To detect interference of the tool flank surface, a corresponding formula must be obtained so that the undetected collision error can be analysed. Figure 5(*a*) illustrates the case when the tool flank surface protrudes into a facet in the protected surface but does not interfere with any endpoints in the facet. In the figure, three endpoints of the facet are located on the cylindrical surface. The radius of the ball-end cutter is r. According to Fig. 5(*b*), the formula is expressed as

$$e_p = r - \sqrt{(r^2 - d^2/4)}$$

Solving for d, we find

$$d = \sqrt{(8re_p - 4e_p^2)}$$

When e_p is small with respect to r, d is approximated as

$$d \sim \sqrt{(8re_p)} \tag{2}$$

The undetected error must be smaller than a user-specified tolerance e when the algorithm to detect interference is applied to discrete points generated from surface subdivision. The maximum side length d of the facets in the polyhedral model is calculated from equation (1) when a cutter protrusion error for the tool-cutting surface is prescribed. The same side length is obtained from equation (2) when the cutter protrusion error caused by the tool flank surface is considered. We proceed to

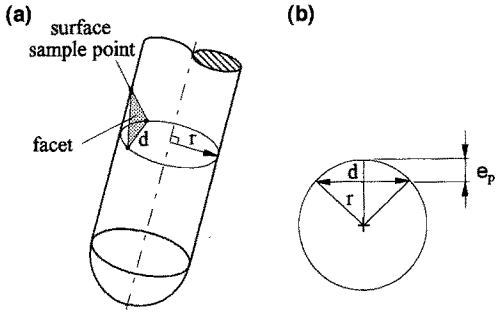

Fig. 5. Tool protrusion error induced by the tool flank surface.

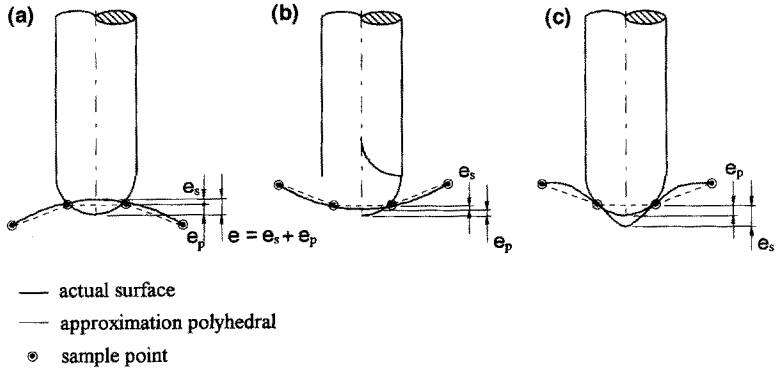

Fig. 4. Possible combinations of surface approximation error and cutter protrusion error [13].

compute the cutter protrusion error induced by the whole tool geometry. The maximal side length d generated from (1) is smaller than that from (2) when a prescribed e_p is substituted into the equations. Consequently, we can choose (1) as the formula to calculate d when the cutter protrusion error is induced by both tool-cutting and flank surfaces.

3.2 Subdivision Procedures

All facets obtained during surface subdivision need further checking even though their side lengths are smaller than d. As e_s also results in the interference detection error, facets obtained according to equation (1) must be subdivided if the combined error is larger than the prescribed tolerance e. The surface subdivision procedures are described as follows:

1. As shown in Fig. 4, the condition $e \geq e_p$ is always valid. We define $e_p = ne$, where $n > 1$ and n is a heuristic parameter that is used to adjust the computation time and approximation result. Substituting $e_p = ne$ into equation (1), we find that $d = \sqrt{(6ren)}$.
2. All tool paths are obtained at the tool-path generation stage. We calculate the length of each tool path and take the average, L. If u iso-parametric curves are chosen to be the guideway of the tool path, we can find a set of v iso-parametric curves which are conjugate to the tool paths. The average length, W, of the set of v iso-parametric curves is thus computed.
3. If a surface patch can be subdivided into equilateral triangles, the number of total discrete points is the minimum [13]. Therefore, each surface patch is first divided into strips which are then divided into equilateral triangles. Here we assume that an equilateral triangle in parametric space corresponds to an equilateral triangle in Cartsian space. This assumption may not be valid in surface regions with large curvatures, but the facets in these regions will be recursively subdivided at a later step. As depicted in Fig. 6, the parameter range of each surface patch is normalised to [0,1] and we take strips from u parameters with fixed intervals Δu. In each strip, we take equilateral triangles from v parameters with fixed intervals. The values of Δv, Δu and Δv are given by

$$\Delta u = \frac{\sqrt{3}d}{2W} \quad \Delta v = \frac{d}{L}$$

4. The approximate patch has been divided into small facets after the above step but some of them may not satisfy the criteria of maximal undetected error. Those facets are further divided at this step. First, the side lengths of each facet are calculated to ensure that every side length is smaller than d. If a side length is larger than d, the facet that contains it is subdivided barycentrically, as shown in Fig. 7. Note that we take the parametric midpoint of the side whose length is larger than d. After this subdivision, every side length is smaller than d. The surface approximation error e_s in the facet with small curvature is almost zero and the surface subdivision process is completed because the equation $e_s + e_p < e$ is satisfied. On the other hand, the facet which locates on a surface region with large curvature must be further divided so that the undetected error is smaller than e. First, e_s is estimated for each side of a facet. Secondly, the longest side length is taken as d to calculate e_p. In the case shown in Fig. 4(*c*), the equation $e_s < e$ should be satisfied; otherwise, $e_s < e - e_p$ must be valid. If the criteria of maximum undetected error is not satisfied for a side, this side is subdivided into two sides as illustrated in Fig. 7.

All protected surfaces are subdivided into a set of sample points to detect interference according to the above subdivision procedures. Figure 8 shows the subdivision result of test examples.

3.3 Voxel Model of Sample Points

For a given cutter location point, only a small number of the sample points can interfere with the cutter. A special data structure called a 3D voxel model is established so that the possible sample points with interference can be discovered quickly. First, points generated by subdivision are sorted into voxels with regular (x,z)-spacing. These voxels are considered "buckets" containing sample points. Next, the tool geometry is projected onto the (x,z)-plane and the voxels that cover the projection range are obtained. All sample points in those voxels must be examined for interference detection. In five-axis machining, the projection profile of the cutter geometry onto the (x,z)-plane cannot be described by analytic forms such as line, arc or quadratic curves. Therefore, instead of the exact projection profile of the cutter, we calculate only its bounding box. Figure 9 illustrates a general APT cutter at a specified cutter location and the coordinate system. Assume the unit

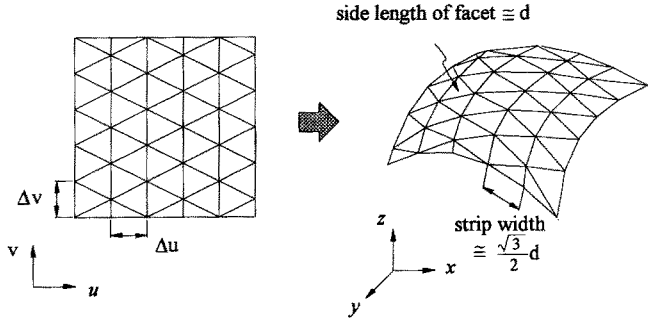

Fig. 6. Surface patch is subdivided into equilateral triangles.

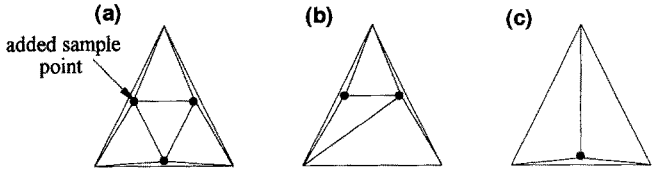

Fig. 7. Subdivision of facet when the criteria of maximal undetected error are not satisfied for (*a*) three sides, (*b*) two sides, and (*c*) one side.

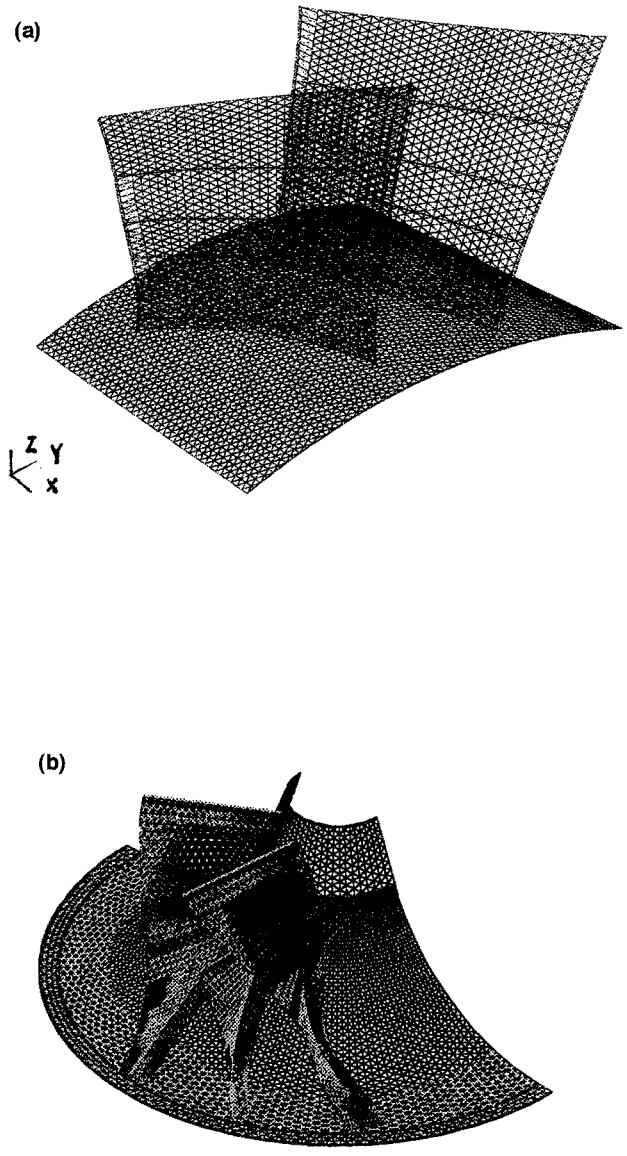

Fig. 8. Subdivision results of test examples.

vector of the tool axis is **n**, the tool bottom point is **b** and the tool end point is **e**. There is a symmetric plane **P** of cutter geometry, at any instant, which contains both **n** and **b**. In addition, its normal vector **m** is equal to the cross-product of the tool axis orientation and the projection direction, that is, $\mathbf{m} = \mathbf{n} \times (0, 1, 0)$. To find the bounding box of the cutter projection, we first calculate the two assistant profiles $\mathbf{c}_1$ and $\mathbf{c}_2$ of the cutter. $\mathbf{c}_1$ and $\mathbf{c}_2$ are two circular profiles in 3D space with direction vector **n**. They pass **b** and **e**, respectively, and their radii are equal to **R**. Since **P** is a symmetric plane of the cutter, **P** intersects both $\mathbf{c}_1$ and $\mathbf{c}_2$ at two points. Assume the corresponding intersection points with $\mathbf{c}_1$ and $\mathbf{c}_2$ are $\mathbf{p}_1$, $\mathbf{p}_2$ and $\mathbf{p}_3$, $\mathbf{p}_4$, respectively, as shown in Fig. 9. Projecting $\mathbf{c}_1$, $\mathbf{c}_2$ and the intersection points onto the (x,z)-plane, we obtain Fig. 10. Assume $\mathbf{p}_1$ and $\mathbf{p}_4$ are the outermost points along the direction **n** of points $\mathbf{p}_1$, $\mathbf{p}_2$, $\mathbf{p}_3$ and $\mathbf{p}_4$. Then, the bounding box of the cutter projection contains four vertices $\mathbf{a}_1$, $\mathbf{a}_2$, $\mathbf{a}_3$ and $\mathbf{a}_4$ which are expressed by

$$\mathbf{a}_1 = \mathbf{p}_1 + R\left(-\frac{n_z}{n_x}\sqrt{\left(\frac{n_x^2}{n_x^2+n_z^2}\right)}, +\sqrt{\left(\frac{n_x^2}{n_x^2+n_z^2}\right)}\right)$$

$$\mathbf{a}_2 = \mathbf{p}_1 + R\left(+\frac{n_z}{n_x}\sqrt{\left(\frac{n_x^2}{n_x^2+n_z^2}\right)}, -\sqrt{\left(\frac{n_x^2}{n_x^2+n_z^2}\right)}\right)$$

$$\mathbf{a}_3 = \mathbf{p}_4 + R\left(-\frac{n_z}{n_x}\sqrt{\left(\frac{n_x^2}{n_x^2+n_z^2}\right)}, +\sqrt{\left(\frac{n_x^2}{n_x^2+n_z^2}\right)}\right)$$

$$\mathbf{a}_4 = \mathbf{p}_4 + R\left(+\frac{n_z}{n_x}\sqrt{\left(\frac{n_x^2}{n_x^2+n_z^2}\right)}, -\sqrt{\left(\frac{n_x^2}{n_x^2+n_z^2}\right)}\right)$$

where $\mathbf{n} = (n_x, n_y, n_z)$. Consequently, we can find the bounding box of the cutter projection in the (x,z)-plane, which consists of the four line segments joining $\mathbf{a}_1$, $\mathbf{a}_2$, $\mathbf{a}_3$, and $\mathbf{a}_4$. The voxels that contain the bounding box can thus be easily found. Only the sample points in these voxels need further interference detection.

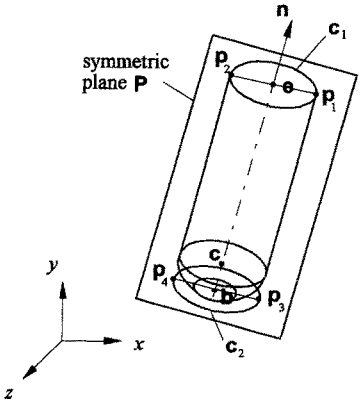

Fig. 9. A general APT cutter and its symmetric plane **P**.

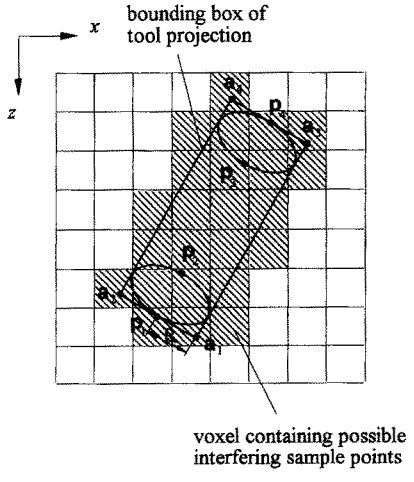

Fig. 10. Bounding box of tool projection on the (x,y)-plane.

4. Interference Detection

For a general APT cutter, it is assumed that the cutter consists of two parts, its cutting surface and its flank part. The flank part is generally a cylindrical surface. If the tool-holding part is included in interference detection, the flank surface can comprise several cylindrical surfaces with varied radii. The cutting surface is represented as a symmetrical surface of revolution, which means that the cross-section at any specific position along the cutter axis has a given radius. Therefore, the whole-tool geometry can be expressed as a function of position along the cutter axis. To simplify the explanation, we assume that the cutter consists of only two parts. The flank part is a cylindrical surface of radius R and the cutting surface is described as $r(h)$, where h is the distance from $\mathbf{b}$ along the tool axis. Consequently, a point $\mathbf{p}$ on the tool axis can be expressed by $\mathbf{p} = \mathbf{b} + h\cdot\mathbf{n}$. The radius r along the tool axis is given by

$$0 \le h < D_c, \qquad r = r(h)$$
$$D_c \le h \le D_c + D_f, \quad r = R$$

where D_c is the length of the cutting surface and D_f is the length of the flank surface along the tool axis. Figure 11 shows a cutter at a given tool position ($\mathbf{b}$, $\mathbf{n}$) and a sample point $\mathbf{s}$ in 3D space. The projection point of $\mathbf{s}$ onto the tool axis is $\mathbf{p}$. Here we define a connecting vector $\mathbf{sp}$, which is used to determine the relative position between $\mathbf{s}$ and the tool at ($\mathbf{b}$, $\mathbf{n}$). $|\mathbf{sp}|$ is the least distance from $\mathbf{s}$ to the tool axis. If the height h of $\mathbf{p}$ along the tool axis is within D_c, the cutting surface is considered to cause an interference. If h is in the range from D_c to D_f, the associated tool geometry is a cylindrical surface with radius R. Note that the tool-holding parts can be included for interference avoidance if they can be described with cylindrical surfaces of varied radii. The parameter h of the projected point $\mathbf{p}$ in the tool axis is given by

$$h = \frac{(e_x - b_x)(s_x - b_x) + (e_y - b_y)(s_y - b_y) + (e_z - b_z)(s_z - b_z)}{(e_x - b_x)^2 + (e_y - b_y)^2 + (e_z - b_z)^2}$$

for which the tool bottom point $\mathbf{b} = (b_x, b_y, b_z)$, tool endpoint $\mathbf{e} = (e_x, e_y, e_z)$, and surface sample point $\mathbf{s} = (s_x, s_y, s_z)$. Consequently, interference occurs when

$$0 \le h < D_c \qquad \text{and } |\mathbf{ps}|^2 < r^2(h) \tag{3a}$$
$$D_c \le h \le D_c + D_f \text{ and } |\mathbf{ps}|^2 < R^2 \tag{3b}$$

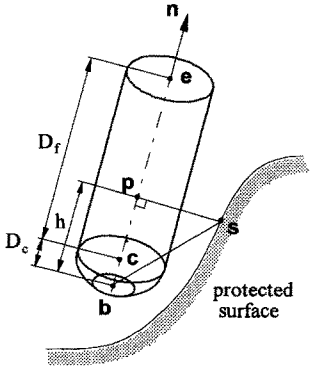

Fig. 11. Smallest distance from a sample point to a given tool axis.

We use the square of the length instead of the actual distance in the above equations as it requires less computation. Equation (3) is the criterion for interference detection.

In five-axis machining, the tool motion between any two cutter locations can interfere with the protected surfaces. However, intensive computation is required when the mathematical description of the tool-swept volume is used directly to test interference. Modifications are consequently made in the work so that the interference criterion is also applicable to tool motions between the cutter location points. Figure 12 illustrates two successive cutter locations ($\mathbf{b}_1$, $\mathbf{n}_1$) and ($\mathbf{b}_2$, $\mathbf{n}_2$), in five-axis machining. The description of the tool motion between the two cutter locations is interpolated from ($\mathbf{b}_1$, $\mathbf{n}_1$) and ($\mathbf{b}_2$, $\mathbf{n}_2$). If we assume that linear interpolation is employed, the tool motions are described as

$$\mathbf{b}(t) = \mathbf{b}_1 + t\,(\mathbf{b}_2 - \mathbf{b}_1)$$
$$\mathbf{n}(t) = \mathbf{n}_1 + t\,(\mathbf{n}_2 - \mathbf{n}_1)$$

in which t is the interpolation parameter and $0 \le t \le 1$. Instead of testing interference over the continuous interval, a set of discrete points $0 \le t_1 \le t_2 \le t_3 \le \ldots \le t_{n-1} \le 1$ is chosen for interference detection. Therefore, the continuous tool-swept volume is replaced by the discrete tool positions ($\mathbf{b}(0)$, $\mathbf{n}(0)$), ($\mathbf{b}(t_1)$), $\mathbf{n}(t_1)$), ($\mathbf{b}(t_2)$, $\mathbf{n}(t_2)$), . . ., ($\mathbf{b}(t_{n-1})$, $\mathbf{n}(t_{n-1})$), ($\mathbf{b}(1)$, $\mathbf{n}(1)$) between the two cutter location points. The interference detection criterion, equation (3), is thus executed at the discrete tool positions. The number of sample positions is a compromise between computation time and accuracy. In the most simplified condition, only the tool positions at $t = 0$ and $t = 1$ are examined for interference and the tool motion between the cutter locations is ignored.

5. Implementation and Results

The proposed algorithms are implemented in the SpringSolid system using the C++ language. This system was developed in the CAD laboratory of the Department of Mechanical Engineering, National Taiwan University. A turbine part (shown in Fig. 13) is used as a test example to demonstrate the feasibility of the work. This part consists of a base cone surface and fifteen blades of free form surfaces. Since the distance between two adjacent blades is small and the blade surfaces have twist regions, cutting tools are very likely to cause interferences in the machining process, which contains five machining operations including rough milling, semi-finish milling of the blade surfaces, finish milling of the blade surfaces, finish milling of the cone surface and rounding operations. A flat-end cutter of 12-mm radius, a ball-end cutter of 5-mm radius and with a 3-degree taper angle and a ball-end cutter of 2-mm radius are used in the machining process.

In the test examples, the intersection curves between the consecutive planes with descending z-values, and the blades surface, are the guiding curves for tool paths in the finish and semi-finish milling operations. Each tool path is subdivided into discrete points according to the prescribed machining tolerance which are 0.005-mm sideways tolerance and 0.005-mm forward tolerance. Those discrete points are specifically

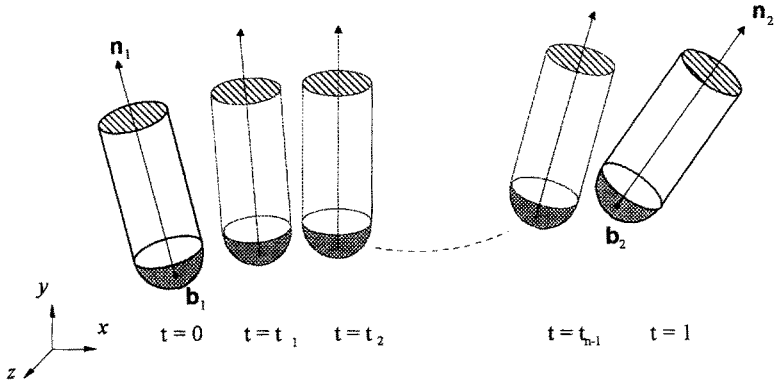

Fig. 12. Discrete checked positions between two cutter locations.

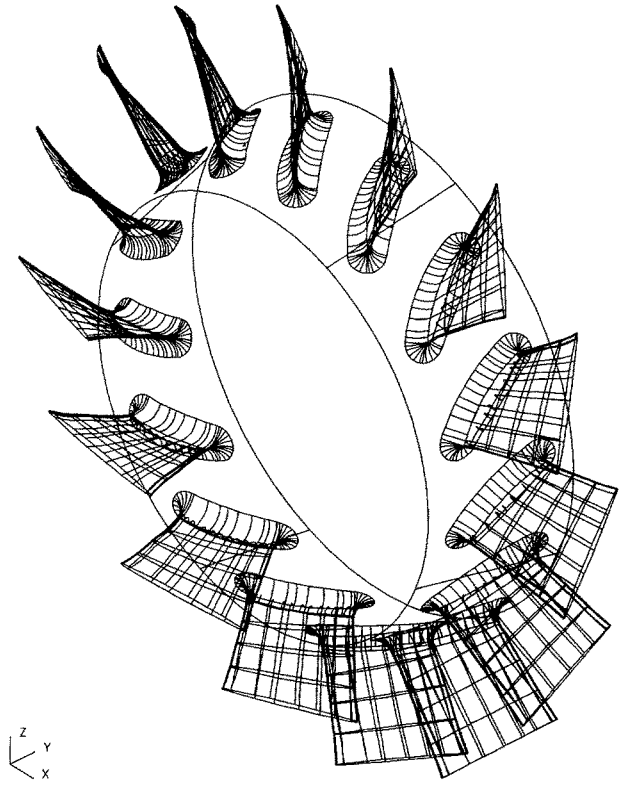

Fig. 13. A turbine workpart is used as the test example of interference detection.

the cutter contact points on the machined surfaces. The contact of the ball-end cutter and the blades is the contact of the side cutting edge. The tool orientation has linear variations from a tilt angle of 90° on the top to a tilt angle of 75° on the bottom of the blades. For the definition of the tilt angle refer to [10].

Figure 14(*a*) illustrates the occurrence of tool collision between the ball-end cutter with a 5-mm radius at a cutter contact point. The tolerance of interference detection is 0.01 mm. Note that the crosses indicate the sample points of the blade surface at which collision occurs. Figure 14(*b*) shows the tool causes no collision at the new cutter location, which is automatically generated by our interference correction algor-

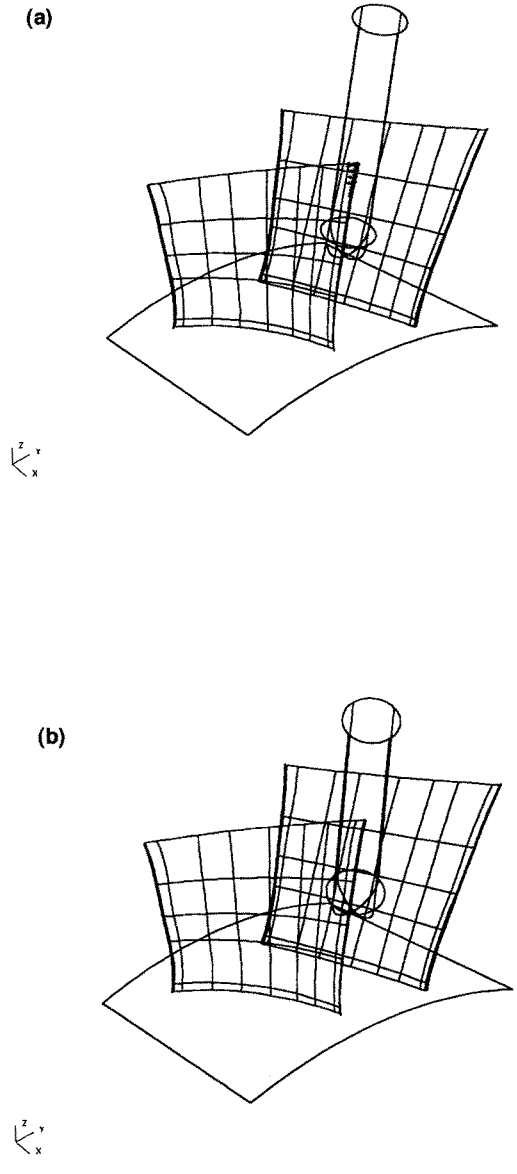

Fig. 14. (*a*) The occurrence of tool collision between a ball-end cutter and the blade surface of the test example. (*b*) The ball-end cutter in the new cutter location causes no collision with the test example.

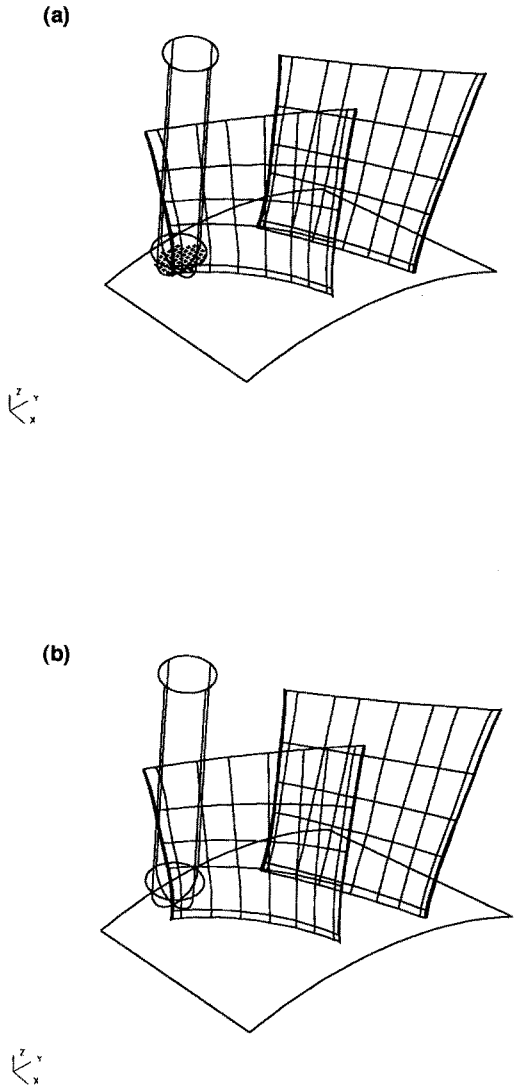

Fig. 15. (*a*) The occurrence of tool overcut between a ball-end cutter and the bottom surface of the test example. (*b*) The ball-end cutter in the new cutter location causes no overcut with the test example.

ithms [10]. Figure 15(*a*) indicates the overcut of the same ball-end cutter on the base cone surface. The crosses indicate the sample points of the bottom surface with overcut. Figure 15(*b*) is the result of interference correction.

6. Conclusions

We present a systematic approach for tool-path verification in five-axis machining of sculptured surfaces. A maximum undetected error is ensured within a user-specified tolerance. Interference which occurs across multiple surfaces can be found with the approach. In addition, the tool paths can be verified by consideration of the whole-tool geometry. The implementation of the proposed algorithms demonstrates its feasibility and flexibility. However, the computation efficiency of the approach needs more analysis and its capabilities for interference correction deserve further research.

References

1. H. Henning, "Fünfachsiges NC-Fräsen gekrümmter Flächen", dissertation, University of Stuttgart, Germany, 1975 (in German).
2. H. Damsohn, "Fünfachsiges NC-Fräsen, ein Beitrag zur Technologie Teileprogrammierung und Postprozessorverarbeitung", dissertation, University of Stuttgart, Germany, 1976 (in German).
3. G. B. Vickers and K. W. Guan, "Ball-mills versus end-mills for curved surface machining", *ASME Journal of Engineering for Industry*, **111**, pp. 22–26, February 1989.
4. W. T. Lei, "Flächenorientierte Steuerdatenaufbereitungen für das fünfachsiges Fräsen", dissertation, University of Stuttgart, Germany, 1992 (in German).
5. X. S. Li and R. B. Jerard, "5-axis machining of sculptured surfaces with a flat-end cutter", *Computer-Aided Design*, **26**(3), pp. 165–178, 1994.
6. K. Y. Chang and E. D. Goodman, "A method for NC toolpath interference detection for a multi-axis milling system", *ASME Conference of Control Manufacturing Processes*, pp. 23–30, 1991.
7. W. P. Wang and K. K. Wang, "Geometric modeling for swept volume of moving solid", *IEEE CG&A*, **6**(12), pp. 8–17, December 1986.
8. J. P. Kruth and P. Klewais, "Optimization and dynamic adaptation of the cutter inclination during five-axis milling of sculptured surfaces", *Annals of the CIRP*, **43**(1), pp. 443–448, 1994.
9. W. P. Wang, "Solid modeling for optimization metal removal of three-dimensional NC end milling", *Journal of Manufacturing Systems*, **7**(1), pp. 57–65, 1987.
10. C. F. You and C. H. Chu, "A systematic approach to correct tool interference in five-axis machining". Proceedings of the Twelfth National Conference of CSME, pp 655–664, 1995.
11. B. K. Choi and C. S. Jun, "Ball-end cutter interference avoidance in NC machining of sculptured surfaces", *Computer-Aided Design*, **21**(6), pp. 371–378, 1989.
12. J. H. Oliver, D. A. Wysocki and E. D. Goodman, "Gouge detection algorithms for sculptured surface NC generation", *ASME Journal of Engineering for Industry*, **115**, pp. 139–144, 1993.
13. R. B. Jerard, R. L. Drysdale, K. Hauck and B. Schaudt, "Method for detecting errors in numerically controlled machining of sculptured surfaces", *IEEE Computer Graphics and Applications*, **9**(1), pp. 26–39. 1989.
14. R. L. Drysdale and R. B. Jerard, "Discrete simulation of NC machining", *Proceedings ACM Symposium on Computational Geometry, New York*, pp. 126–135, 1987.
15. R. M. Aretz, "Kollisionsvermeidung bei der Fertigung von Freiformflächen", Part 2, *CAD-CAM Report*, **5**, pp. 114–124, 1990 (in German).
16. U. A. Sungurtekin and H. B. Voelcker, "Graphical simulation and automatic verification NC machining programs", *Proceedings of IEEE International Conference on Robotics and Automation*, **3**, pp. 156–165, 1986.
17. Y. Takeuchi and T. Watanabe, "Generation of 5-axis control collision-free tool path and postprocessing for NC data", *Annals of the CIRP*, **41**(1), pp. 539–542, 1992.